Gaze Estimation as a Framework for Iris Liveness Detection

Ioannis Rigas
Texas State University
601 University Drive, San Marcos, TX 78666
rigas@txstate.edu

Oleg V. Komogortsev
Texas State University
601 University Drive, San Marcos, TX 78666
ok11@txstate.edu

Abstract

This work investigates the possibility of detecting iris print-attacks via the analysis of a number of gaze-related features acquired in a process of eye tracking. Gaze estimation algorithms employ models based on the physical structure and function of the eye, providing thus a number of salient features that can be potentially employed for the detection of spoofing print-attacks. In our study, a combined dataset was assembled for the investigation of these features, consisting of eye movement recordings and the corresponding iris images collected from 100 subjects. The collected iris images were utilized in direct implementation of iris print-attacks against an eye tracking device. We developed a methodology for the detection of spoof indicative artifacts in the recorded signals, and fed the extracted features from the "live" and "spoof" eye signals into a two-class SVM classifier. The obtained results indicate a best correct classification rate (CCR) of 95.7%. Furthermore, we demonstrate the moderate decrease in liveness detection rates during subsampling of the eye movement signal to frequencies as low as 15 Hz. This result indicates the usefulness of running gaze estimation algorithms on existing iris recognition devices where such sampling frequency rate is common.

1. Introduction

For a long time the research concerning well-established biometric modalities such as the fingerprints, iris, and face, moved towards a march for an optimization of the algorithmic techniques used during the representation and comparison of biometric templates. In this way, biometric systems gradually evolved in their current state of performance, capable of delivering impressively high accuracy rates, and performing biometric template extraction and matching speedily. In spite of the remarkable advances in the field, a thorny issue has been reported throughout the history of automated personal recognition, regarding the insufficient resistance of systems to spoofing attacks using counterfeits of the genuine biometric templates [1], [2], [3], [4]. An additional alarming concern is the easiness with what successful replicas can be constructed by using common materials, e.g. printing paper (iris and face) and gelatin (fingerprints). As a result, the development of techniques for the detection of such attacks appears as a compelling research task in the field of biometrics. The necessity for effective countermeasures is further emphasized considering the current trend of biometric technologies to migrate from the relatively controlled environments of military and government agencies, to personal appliances (e.g. smartphones, cars) and everyday transactions (banks, shopping etc.).

The term *liveness detection* can be generally used to describe an ensemble of research techniques aiming at the recognition of signals generated from valid biometric templates ("live" samples) and the corresponding artificial imitations ("spoof" samples). In the field of iris biometrics, one of the first systematic attempts for the suggestion of countermeasures against direct iris spoofing print-attacks was presented in [5]. The techniques presented in that work included analysis of the frequency spectrum of iris images, examination of the eye reflectance properties for controlled static light patterns, and exploration of pupil dynamics. Characteristics of eye pupil were the main topic of research in the work presented in [6]. In this case, the proposed framework involved various computational techniques for the quantification of iris patch differences, and for the comparison of iris and pupil diameters. An approach based on the representation of texture using Local Binary Patterns (LBPs) was proposed in [7]. The suggested method was evaluated under a more sophisticated spoofing attack scenario, implemented with the use of printed contact lenses. A different route was followed in [8], with the presented methodology targeting on the detection of distinctive distortions in image quality, arising during the capturing procedure. Some characteristic examples of this kind of distortions involve focus features, motion blur, and occlusion artifacts. The liveness detection framework that was proposed in [9] was based on the discovery of "alien" frequencies in the spectrum of fake iris samples. The technique was evaluated using a large database of iris printouts constructed under controlled quality conditions.

Recently, in [10], biometric techniques based on eye movements were evaluated for eye liveness detection, in a scenario simulating the attack with a mechanical replica of

the human eye. It should also be noticed an accelerated urgency in researching liveness detection methods, with the organization of liveness detection competitions regarding iris recognition [11] and other prominent biometric modalities [12], [13].

1.1. Motivation

In the present research work, we explore the capabilities of an iris print-attack detection framework based on the process of gaze estimation. There are several studies (e.g. [3], [14]) demonstrating that direct iris print-attacks are easy to implement and remarkably efficient. During such an attack, an image of a real iris is obtained, printed with a high quality printer, and presented in front of the image sensor of an iris scanner. The printed image may have a hole in the place of the pupil, in order to by-pass the corneal reflection control check usually made by an iris-scanning device. It should be noted that an iris scanner and an eye tracking system essentially employ similar hardware, i.e., image sensor and an IR light, thus making it possible to do iris and eye movement-driven biometrics on the same device [15]. The hole in the printed image of the iris allows for the corneal reflection movement to be recorded, making possible a print-attack even against sophisticated biometric systems that incorporate eye tracking capabilities.

This possibility, of using a very simple replica (printed image) to spoof an iris recognition device running eye tracking algorithms, motivated us to develop a methodology to detect such spoofing attempts. This work presents for the first time experimental data involving a practical print-attack spoofing scenario, performed against an eye tracking device. Our contribution may be summarized as follows:

1) We provide a theoretical description of eye gaze estimation process based on Pupil Center Corneal Reflection (PCCR) technique, and present the possible artifacts that may arise to the recorded eye movement signals during an iris print-attack.

2) We develop a methodology for the detection of print-attacks, based on the analysis of the generated eye movement signal distortions.

3) We evaluate performance of the proposed method against actual print-attacks. A two-stage experiment was organized, involving "live" eye gaze and iris image recordings from 100 subjects, and the utilization of the respective printed iris images for performing attacks against an eye tracking device, that simulated iris scanner with incorporated eye movement detection abilities.

4) We demonstrate that the reduction of the temporal sampling rate of eye image capturing to a level common to existing iris biometric systems brings about only a small decrease in the detection rates for the spoof attack. This result is supporting a possible incorporation of eye tracking features in a multi-modal iris recognition system.

2. Gaze Estimation in the Case of Print-Attack Iris Spoofing

2.1. Theoretic Framework of Gaze Estimation

In this section we provide an overview of the theoretical background that describes gaze estimation for the general case of a Pupil Center Corneal Reflection (PCCR) eye tracking system. We decided to focus on PCCR technique due to its widespread adoption in the modern eye tracking equipment, given its favorable characteristics regarding accuracy and operational stability. A comprehensive survey describing different eye-gaze models and techniques can be found in [16].

We may define the Point of Gaze (POG) as the intersection of the visual axes of an observer eyes with the observed stimulus. Estimation of POG may be accomplished with the use of one or more light sources, and one or more cameras typically operating in the infrared domain. An increasing number of light sources and/or capturing cameras leads to an equivalent increase in the degrees of freedom allowed for head movements. Given the fact that the visual axis and the optic axis do not coincide in the human visual system, gaze estimation is implemented in two stages: a) estimation of the optic axis using the optical geometry of the eye tracking setting and eye properties, and b) reconstruction of the visual axis from the estimated optic axis using only eye properties.

The adopted mathematical formulation involved during gaze estimation is based on the general framework described in [17]. In Figure 1, we present a schematic depicting the configuration that can be used for the estimation of POG, for the simple case of one light source and one camera.

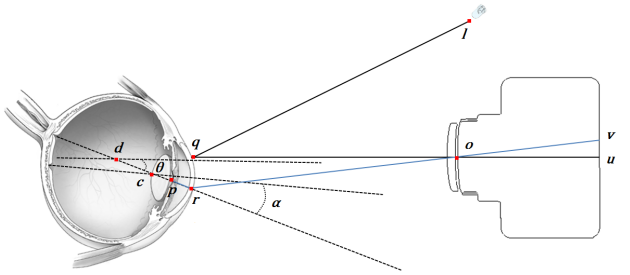

l: light source
q: point of reflection
r: point of refraction
p: pupil center
c: center of corneal curvature
d: center of eye rotation
v: image of pupil center
u: image of corneal reflection
o: nodal point of the camera
θ: angle between optic axis and horizontal plane
α: angle between optic axis and visual axis

Figure 1: Diagram of the gaze estimation configuration for a PCCR based system.

Since the first step for the estimation of POG requires the computation of optic axis, we need to find two points that the axis crosses, and calculate their coordinate vectors. From Figure 1, we may observe that the optic axis crosses the center of the corneal curvature (***c***) and the pupil center

($\boldsymbol{p}$). An eye tracking system is able to calculate the coordinate vectors of these two points by analyzing the captured images of the corneal reflection center ($\boldsymbol{u}$) and the center of the pupil ($\boldsymbol{v}$), and by employing the optical geometry and the properties of human eye structure. Let us denote K the distance between the pupil center ($\boldsymbol{p}$) and the center of the corneal curvature ($\boldsymbol{c}$). Then, we may extract an equation connecting these two points as:

$$\|\boldsymbol{p} - \boldsymbol{c}\| = K \quad (1)$$

The exact value for parameter K depends on the eye structure, and can be calculated from a calibration procedure occurring prior to the main gaze estimation process.

Since $\boldsymbol{p}$ and $\boldsymbol{c}$ represent coordinate vectors, a set of additional equations are needed for their estimation. Optical geometry of the configuration used for gaze estimation (Figure 1) can be employed for the extraction of the remaining equations needed to determine $\boldsymbol{p}$ and $\boldsymbol{c}$. The condition that a ray of light coming from a point source $\boldsymbol{l}$ is reflected at a point $\boldsymbol{q}$ of the corneal surface can be written:

$$\|\boldsymbol{q} - \boldsymbol{c}\| = R \quad (2)$$

with R being the radius of the hypothetical spherical mirror representing the cornea. As in the case of K, this parameter can be estimated through the calibration procedure. In an analogous manner, the condition that a ray of light coming from the center of the pupil $\boldsymbol{p}$ is refracted at a point $\boldsymbol{r}$ of the corneal curvature is formulated as:

$$\|\boldsymbol{r} - \boldsymbol{c}\| = R \quad (3)$$

In addition, points $\boldsymbol{q}$ and $\boldsymbol{r}$ are related with the captured images of the corneal reflection center $\boldsymbol{u}$ and the refracted ray from the pupil center $\boldsymbol{v}$ respectively, through the set of parametric equations:

$$\boldsymbol{q} = \boldsymbol{o} + k_q(\boldsymbol{o} - \boldsymbol{u}) \quad (4)$$

$$\boldsymbol{r} = \boldsymbol{o} + k_r(\boldsymbol{o} - \boldsymbol{v}) \quad (5)$$

with k_q, k_r denoting configuration dependent parameters, and $\boldsymbol{o}$ representing the nodal point of the camera. The laws of optic reflection and refraction may be employed for the extraction of the auxiliary equations needed to solve the system of equations (1) to (5) (see [17] for extended details), leading thus to the full estimation of the optic axis.

Reconstruction of the visual axis is independent of the specific eye tracking configuration. Its orientation can be determined by calculating the relative angle $\boldsymbol{\alpha}$ formed with the optic axis, with regard to angle $\boldsymbol{\theta}$, which is the angle between optic axis and the horizontal line crossing the center of eye rotation $\boldsymbol{d}$. Both angles depend exclusively on the observer's eye structure, and they can be computed via the calibration procedure. With the orientation of the visual axis estimated, its reconstruction may be completed with the determination of the coordinates of a point that it crosses, which—in our case—is the already estimated center of the corneal curvature $\boldsymbol{c}$ (see Figure1).

2.2. Gaze Signal Distortions Appearing during Iris Print-Attack Spoofing

In the case of an iris print-attack there are several inconsistencies that affect the POG estimation procedure. The most important of them is the atypical relative positioning of the corneal reflection and the pupil center. Specifically, whereas for a "live" moving eye both the corneal reflection and the pupil center move, in the case of an iris printout the corneal reflection can still move but the pupil center appears to be stationary. Consequently, the relative positions of the pupil and corneal reflection centers would be abnormal compared to the case of a "live" eye. Another deficiency concerns the eye-structure parameters (e.g. R, K) that are estimated during the calibration procedure. As we will explain below, during a print-attack the calculated values for these parameters do not follow the typical range corresponding to "live" eyes. Given their incorporation during visual axis reconstruction and POG estimation, they can serve as an additional source of distortion appearing in the captured signals.

In Figure 2, we demonstrate the unnatural behavior of the "spoof" eye during a print-attack, relative to the "live" eye. In both cases, a fixation has been performed to the same point, 3.5° above the primary eye position (eye looking straight ahead). In the case of a "live" eye, both the corneal reflection and the pupil center changed their positions. On the contrast, for the "spoof" eye the pupil boundary is fixed, and thus the pupil center appears to stay in the same position. Both the inconsistent behavior induced by the functional differences of a printed eye replica, and the qualitative inferiority of an iris printout, are translated into a number of signal distortions that can be detected in the corresponding eye movement recordings.

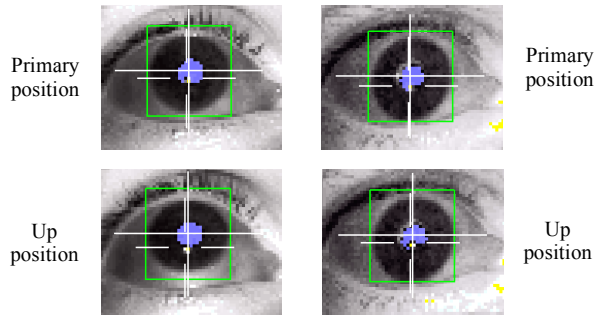

Figure 2: Differences in the relative positioning of the corneal reflection and the pupil center, in the case of (a) a "live" eye and (b) a "spoof" eye.

1) Position Offsets

The most conspicuous distortion appearing in gaze signals recorded during a print-attack, is the presence of position offsets due to the apparent unnatural movement of the center of the corneal reflection relative to the pupil center. Examples of such artifacts are depicted in Figure 3.

The two factors that modulate the exact form of these distortions are the eye-structure parameters—calculated during the calibration procedure—and the mechanics of the gaze estimation process. During a typical eye tracking calibration procedure a subject looks at a set of predefined points (usually nine or five), placed at fixed locations. By solving a set of equations that include linear and non-linear terms a mapping is achieved, leading to the determination of several eye-structure specific parameters that can be used during the estimation of future gaze locations (more details regarding the calibration process for the eye tracking hardware we employed are provided in [18]). Although values of the parameters may vary from person to person (subject-specific), typically they lie on a bounded surface in case of a "live" eye [17]. The structural and functional inconsistencies during an iris print-attack result in the generation of a mapping (and thus calculation of the related parameters) that does not fit to that of a "live" eye. Since the calculated eye-structure parameters are subsequently incorporated in the gaze estimation equations (1) to (3), and used during the reconstruction of visual axis (angle $\boldsymbol{a}$), they co-modulate position distortions in the recorded signals. Even for a theoretically infallible calibration procedure though, the creation of position offsets would be inevitable. Regardless of the validity of the calculated eye-specific parameters, in the case of a print-attack the image of pupil center $\boldsymbol{v}$ will always appear misplaced relative to the respective image of the corneal reflection center $\boldsymbol{u}$. This inherent inconsistency is propagated through equations (4) and (5) to the rest equations used to estimate POG, and in turn is translated to position offsets in the captured signal.

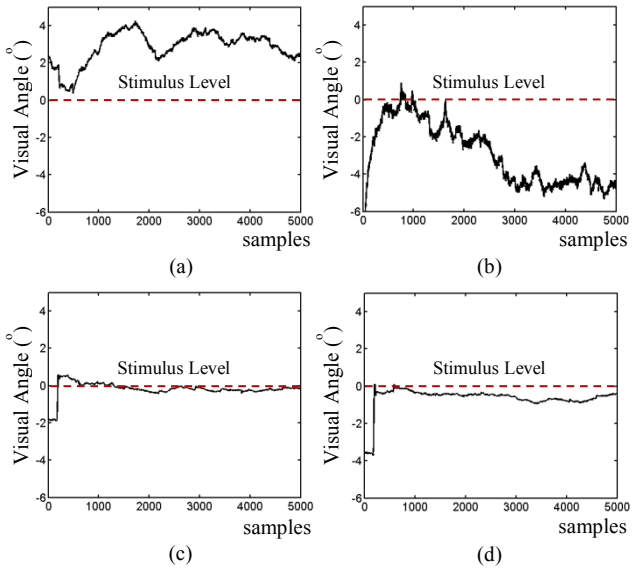

Figure 3: (a)-(b) Position offsets appearing in signals captured during an iris print-attack in comparison to (c)-(d) normal signals recorded from "live" eyes.

2) Local Amplitude Distortions and Noise Artifacts

The structural differences of an iris printout compared to the real eye affect not only the global characteristics of the recorded gaze signals but also their local amplitude levels. Gaze estimation inaccuracies during eye micro-movements and the incorrect models built during calibration, can result in the appearance of unnatural variability of local amplitude levels within the recorded signal. An example of this phenomenon may be observed in Figure 4. The solid lines mark the different amplitude levels in case of a "live" and a "spoof" signal. In addition, the inevitable qualitative deficiencies of an iris printout (no moisture, different surface, fitted hole not attached to the pupil), are further contributing to the appearance of enhanced noise artifacts in the "spoof" signals (Figure 4, dashed lines).

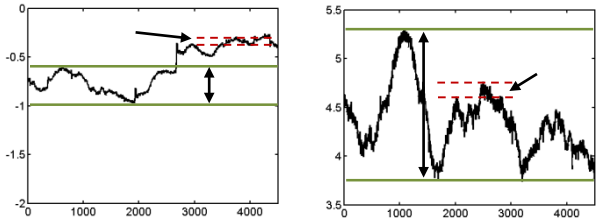

3) Signal Invalidity

Lastly, the aforementioned sources of artifacts can be considered responsible for the occasionally larger degree of eye movement signal loss in the case of a print-attack. This loss usually occurs due to blinks, eye moisture, and squinting, but in the case of a spoof replica presentation it occurs due to the eye tracking equipment inability to extract necessary features from the image for gaze estimation.

3. Liveness Detection Features

The method that we developed for the detection of the spoof indicative distortions arising during a print-attack, was inspired by the Complex Eye Movement (CEM) Biometrics framework, presented in [19]. In the current approach, instead of identifying fixations and saccades in an eye movement recording, we perform a finer decomposition of the eye movement signal into a set of elementary units consisted of eye micro-movements. In the sequence, we use the formed signal units in order to calculate statistical features that represent position and amplitude level related properties. The extracted features are employed for the detection of signals that arise from an iris print-attack, and their separation from the valid ones.

The initial decomposition of a recorded signal is performed using the Velocity Threshold Identification

(I-VT) technique, described in [20]. This algorithmic procedure is usually employed for parsing an eye movement signal into sequences of normal fixations and saccades, by calculating the velocities of the recorded samples and comparing them using one or more thresholds. In our methodology, a carefully selected parameterization occurs for the segmentation of the gaze signal into micro-saccades and micro-fixations. Instead of merging the micro-saccadic and micro-fixation parts into individual fixations and saccades, we directly employ the elementary units consisted from eye micro-movements, for the extraction of signal features that incorporate both the global characteristics of the signal, related to position offsets, and the local cues, related to irregular amplitude and noise levels. Based on the signal characteristics, we utilize a velocity threshold of 5°/sec (it should be mentioned that for normal saccades this threshold is about 20°/sec):

$$RawRecording \rightarrow IVT\left(5^{\circ}/sec\right) \rightarrow u_i,\ \ i = 1, \dots, N \qquad (6)$$

with N denoting the number of the elementary units (u_i) generated from the signal decomposition.

In the original implementation of the CEM framework [19], several different primitive features were proposed for the description of fixation and saccade basic properties. From the provided ensemble of characteristics we selected the *Horizontal Fixation Centroid* and the *Vertical Fixation Centroid* features. During the experimental assessment of the possible traits that could be embodied in the developed technique, these specific features proved to be more informative and stable than the others, due to their high correlation with the positional attributes of the two categories of signals ("live"/"spoof"). In order to represent the local position characteristics of every elementary unit u_i, we calculate the centroid for the horizontal (u_hor_i) and vertical (u_ver_i) components:

$$c\_hor_i = \sum_{k=1}^{K} u\_hor_i(k)/K \qquad (7)$$

$$c\_ver_i = \sum_{k=1}^{K} u\_ver_i\,(k)/K \qquad (8)$$

with K denoting the number of discrete samples composing the i^{th} elementary unit. The calculated vectors of centroids are then used for the formation of Liveness Detection Features (LDFs), by concatenating in a common feature vector—consisted of both the horizontal and the vertical components—the average value and the corresponding standard deviation over the centroids of different elementary units u_i. The resulting feature accounts thus both for global position properties (average value term), and for the variability appearing in amplitude levels (standard deviation term). We have:

$$LDF\_hor \rightarrow \{avg(c\_hor_i), std(c\_hor_i)\} \qquad (9)$$

$$LDF\_ver \rightarrow \{avg(c\_ver_i), std(c\_ver_i)\} \qquad (10)$$

The extracted features can be directly used for the detection of gaze signals recorded during an iris print-attack and those generated from live human eyes.

4. Experimental Validation

4.1. Experimental Methodology

In order to evaluate the suggested scheme on the task of liveness detection, we performed a two-stage experiment: in the first stage we constructed a combined database, by recording the eye movements and the iris images from a large number of subjects. In the second stage, we employed the captured iris images to perform iris print-attacks on the eye tracking system that simulated iris scanner with eye tracking capabilities. The complete database that was used during our experiments is publicly available in [1].

4.1.1 Experimental Stimulus

The stimulus used in both experimental stages was a single point placed at a visual angle of 3.5° above the primary eye position (eye staring straight ahead). Subjects were instructed to move their gaze towards this point, and fixate for a total duration of 15 seconds. Selection of this specific stimulus was driven by the necessity to inspect the fundamental properties of the gaze signal during a print-attack. It should be noted that the stationary stimulus represents the most difficult case regarding liveness detection, and can be directly generalized for the case of a stimulus containing excessive motion, where signal distortions are expected to be even worse. A second reason for the chosen scenario is related to the possibility to incorporate the developed scheme in a multi-modal system. In such a system, gaze estimation and iris capturing would be performed simultaneously, and consequently, an excessive movement of the eye would complicate the iris capturing procedure.

4.1.2 Experimental Stage 1: "Live" Eye Recordings

The experiment for collecting the "live" samples was implemented with the participation of 100 subjects (52 male/48 female), ages 18-43 with an average of 22 years (SD 3.7). Every subject was enrolled totally twice, and the time interval between two enrollments was about 30 minutes. During this time, the subject performed other eye tracking tasks with brief periods of rest. The recordings were performed with a monocular EyeLink 1000 eye tracker [21] running at 1000 Hz, with vendor reported spatial accuracy of 0.5°. Data from the left eye were recorded in all experiments. Each subject's head was positioned at a distance of 550 mm from a computer screen (474 mm x 297 mm, resolution 1680 pixels x 1050 pixels), where the stimulus was presented.

The iris images were obtained with a BMT-20 Iris Recognition System [22], capturing high quality iris images with resolution of 640 pixels x 480 pixels. As previously, each subject enrolled a total of two times, yielding a database of 200 unique pairs of iris samples. During the experiments only the left eye iris samples were used.

[1] http://cs.txstate.edu/~ok11/etpad_v1.html

Texas State University institutional review board approved the study, and every participant provided informed consent.

4.1.3 Experimental Stage 2: Print-Attack Recordings

For the second stage of the experiment, print-attack carriers were initially prepared by printing the captured iris templates on matte printer paper, via HP Laserjet 4350dtn gray scale printer, with a resolution of 1200 dpi x 1200 dpi. Selection of matte instead of glossy paper was dictated by the specificity of the implemented experiment, that involved recordings with an eye tracking device. As it was practically verified during our preparatory experimental assessment, the reflectance properties of glossy paper render extremely difficult any capturing of the pupil and/or the corneal reflection. In order to complete the preparation of the attack carriers, we carefully removed the pupil part from every printout, forming thus a hole that allowed corneal reflections to be captured.

Implementation of print-attacks was performed by fitting every iris printout on an "eye patch" mask with a small window, allowing for a steady adjustment of the carrier to the person performing the spoofing attack. In order to ensure that the extracted liveness characteristics depend mainly on the print-attack specific deficiencies and not on inter-person specific features, a subject that did not belong to the formed experimental database was selected to perform the spoofing attacks.

We decided to perform two different spoofing attack scenarios, in order to assess the effectiveness of the proposed scheme to detect distortions that are related both to the calibration stage and to the stimulus presentation stage:

Spoofing Attack Scenario I (SAS-I). In the first attack scenario, the employed eye tracking system is directly attacked using the prepared iris printouts, both during the calibration procedure and during the main gaze recording phase (stimulus presentation stage). Gaze signals that are captured during such an attack, should carry distortions that arise from both sources.

Spoofing Attack Scenario II (SAS-II). In the second attack scenario, the employed eye tracking system is attacked exclusively during the stimulus presentation stage, whereas the calibration procedure is implemented by a valid ("live") eye. This scenario corresponds to the case that the attacker is capable to by-pass the calibration procedure (e.g. the system is pre-calibrated) and perform the spoofing attack directly during the main process.

4.2. Results

4.2.1 Performance Metrics

The feature vectors extracted from the "live" and "spoof" eye recordings are fed into a classification scheme based on a SVM classifier with a Gaussian Radial Basis Function kernel ($\sigma = 1$). Selection of a SVM classifier was decided due to its effectiveness on two-class problems, as the scenario regarding the detection of "spoof" and "live" signals. The following classification performance metrics were employed in order to evaluate the proposed method:

Correct Classification Rate (CCR). CCR is defined as the percentage of correctly classified test samples (either "live" or "spoof") to the total number of test samples.

False Spoof Acceptance Rate (FSAR). FSAR is defined as the percentage of "spoof" test samples that are incorrectly classified as "live".

False Live Rejection Rate (FLRR). FLRR is defined as the percentage of "live" test samples that are incorrectly classified as "spoof". Additionally, we can define True Positive Rate (TPR) = 1 – FLRR.

Equal Error Rate (EER). EER is defined as the point of a Receiver Operating Characteristic (ROC) curve for which FSAR equals FLRR. The following procedure may be performed for the calculation of EER in the case of a SVM classifier: given the condition the two classes under consideration are not completely separable, the distances of the misclassified samples from the optimum separating hyperplane can be employed as "soft-scores". By varying the acceptance threshold for these "soft-scores" a ROC curve can be constructed, making thus possible the determination of EER.

Table 1. Performance rates for spoofing attacks of type SAS-I, SAS-II.

SAS type	*CCR (SD)* %	*FSAR (SD)* %	*FLRR (SD)* %	*ERR* %
SAS-I	93.1 (2.8)	12.1 (5.4)	1.7 (1.9)	4.3 (2.1)
SAS-II	95.7 (2.1)	6.2 (3.2)	2.3 (2.4)	3.8 (1.9)

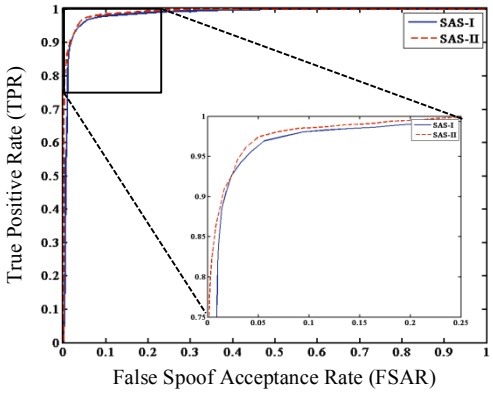

Figure 5: ROC curves for spoofing attacks of types SAS-I, SAS-II.

Table 1 presents the calculated rates for both types of performed spoofing attacks (SAS-I, SAS-II). The demonstrated results were calculated using an 80%-20% training-testing split of sample pools, and the presented results are averages over 100 iterations. In Figure 5, we can

observe the ROC curves constructed with the methodology described above, from which reported values for the EER were determined.

During our experiments, we also decided to evaluate the influence of temporal resolution degradation on the suggested liveness detection scheme. Since the majority of iris scanning equipment operates at sampling frequencies as low as 15 Hz, assessment of our method's behavior in such a range is crucial for a possible incorporation in a system that would capture both modalities (gaze and iris) simultaneously. For this reason, we subsampled both the "live" and "spoof" signals from the initial eye tracking frequency of 1000 Hz to a sampling frequency of 15 Hz. Table 2 demonstrates calculated performances for the scenario involving temporal resolution degradation, for both types of spoofing attacks. Correspondingly, in Figure 6 we present the constructed ROC curves, used for the calculation of EERs.

Table 2. Performance rates for spoofing attacks of type SAS-I, SAS-II, with the signals subsampled at a frequency of 15 Hz.

SAS type	*CCR (SD) %*	*FSAR (SD) %*	*FLRR (SD) %*	*ERR %*
SAS-I	92.7 (2.9)	8.2 (4.7)	6.4 (3.7)	6.6 (2.8)
SAS-II	93.9 (2.4)	6.7 (3.8)	5.4 (3.7)	5.9 (2.7)

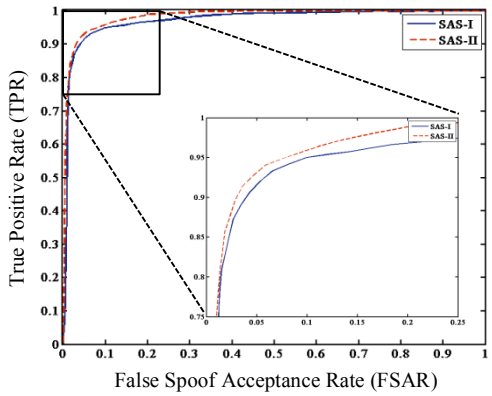

Figure 6: ROC curves for spoofing attacks of types SAS-I, SAS-II, for signals subsampled at a frequency of 15 Hz.

5. Discussion

An inspection of the calculated performance rates and the overall behavior of the suggested scheme, as illustrated from the ROC curves, may reveal the effective separation of the "live" and the "spoof" eye signals, for the performed attack scenarios (SAS-I, SAS-II). The CCR reaches a maximum 95.7%, and the EER is as low as 3.8% (for SAS-II attack). Given the originality of the constructed database, consisted of "live" eye movements and their "spoof" counterparts, we cannot compare our results with other methods directly. However, we should notice that the accuracy of the proposed scheme is similar or in some cases even better than other approaches in the field, e.g., the reported results in [5], ranged from null to 11.1% for FSAR, and from null to 2.8% for FLRR. In [6], where pupil constriction features were explored, the reported CCRs were in the range of 82% to 99.9%. Recently, in [9], the extracted image spectrum features provided a 5% FSAR, for null false rejection of the genuine samples.

A noteworthy observation concerns the superiority (even limited) of SAS-II rates over SAS-I performance. At a first glance, it might be expected to be easier to detect "spoof" signals for SAS-I scenario, since in this case samples are affected both from errors during calibration stage and during stimulus presentation stage. The observed performance differences can be attributed to the increased invalidity of SAS-I samples compared to SAS-II. Specifically, estimation of invalidity for the experimental datasets revealed an average rate of 19.7% for the case of SAS-I, 10% invalidity for samples of SAS-II and 3.5% for the "live" recordings. Consequently, this can be translated in the presence of greater degree of valid information during comparisons for the case of SAS-II, leading on a better separation of the "live" and "spoof" samples.

The results regarding the experiments simulating temporal resolution degradation show only a moderate influence of frequency subsampling on the calculated classification rates. Additionally, it can be observed that the drop in performance is mainly driven by an increase of the FLRR. This behavior reflects the fact that the "live" samples are more susceptible to be influenced by temporal resolution degradation, since their captured patterns are originally more consistent than the "spoof" signals, which are already corrupted by distortions.

We should point out that our research is subject to limitations, which should be accounted during inspection of the results. Our experiments were conducted in a restricted lab environment, minimizing the influence of any external environmental parameters. Furthermore, behavioral aspects might impact generation of gaze patterns, resulting on adverse effects during liveness detection. For example, possible changes in human behavior (e.g. due to tiredness, intoxication etc.) may result in gaze patterns that deviate from normality, thus potentially increasing the FLRR. Finally, it should be noticed that the proposed method was developed based on the characteristics appearing during a paper iris print-attack, which does not guarantee its effectiveness against more sophisticated methods of spoofing.

6. Conclusion

In this work, we presented a research exploring the possibility to utilize gaze estimation as a framework for detecting iris print-attacks on an eye tracking capable iris recognition device. For this reason, we developed a method for the detection of the usual distortions appearing in eye

movement signals in the case of an attack of this type. Furthermore, we practically evaluated our approach by constructing a database composed of eye movement recordings and the corresponding iris images, which were then used for the implementation of direct attacks to an eye tracking system. The results reveal the effectiveness of the proposed scheme to detected print-attack via eye movement signal analysis, even in the case when signal is captured at frequencies as low as 15 Hz. Our future plans include the investigation of more sophisticated signal analysis techniques to improve detection capabilities of our method, and also the inspection of other types of attacks, e.g. iris patterns printed on contact lenses.

Acknowledgements

This work is supported in part by NSF CAREER Grant #CNS-1250718, and NIST Grants #60NANB10D213 and #60NANB12D234. Special gratitude is expressed to Dr. Evgeny Abdulin, Tjitse Miller, Christina Heinich for proctoring eye movement recordings.

References

[1] R. C. Lummis and A. E. Rosenberg, "Test of an Automatic Speaker Verification Method with Intensively Trained Professional Mimics," *The Journal of the Acoustical Society of America,* vol. 51, pp. 131-132, 1972.

[2] T. Matsumoto, H. Matsumoto, K. Yamada, and S. Hoshino, "Impact of artificial "gummy" fingers on fingerprint systems," in *Proc. SPIE 4677, Optical Security and Counterfeit Deterrence Techniques IV, 275*, 2002, pp. 275-289.

[3] V. Ruiz-Albacete, P. Tome-Gonzalez, F. Alonso-Fernandez, J. Galbally, J. Fierrez, and J. Ortega-Garcia, "Direct Attacks Using Fake Images in Iris Verification," in *Biometrics and Identity Management*, B. Schouten, N. C. Juul, A. Drygajlo, and M. Tistarelli, Eds., ed: Springer-Verlag, 2008, pp. 181-190.

[4] Z. Akhtar, G. Fumera, G. Marcialis, and F. Roli, "Robustness Evaluation of Biometric Systems under Spoof Attacks," in *Image Analysis and Processing – ICIAP 2011*. vol. 6978, G. Maino and G. Foresti, Eds., ed: Springer Berlin Heidelberg, 2011, pp. 159-168.

[5] A. Pacut and A. Czajka, "Aliveness Detection for Iris Biometrics," in *Carnahan Conferences Security Technology, Proceedings 2006 40th Annual IEEE International*, 2006, pp. 122-129.

[6] H. Xinyu, T. Changpeng, H. Qi-zhen, A. Tokuta, and Y. Ruigang, "An experimental study of pupil constriction for liveness detection," in *Applications of Computer Vision (WACV), 2013 IEEE Workshop on*, 2013, pp. 252-258.

[7] Z. He, Z. Sun, T. Tan, and Z. Wei, "Efficient Iris Spoof Detection via Boosted Local Binary Patterns," in *Advances in Biometrics*. vol. 5558, M. Tistarelli and M. S. Nixon, Eds., ed: Springer Berlin Heidelberg, 2009, pp. 1080-1090.

[8] J. Galbally, J. Ortiz-Lopez, J. Fierrez, and J. Ortega-Garcia, "Iris liveness detection based on quality related features," in *Biometrics (ICB), 2012 5th IAPR International Conference on*, 2012, pp. 271-276.

[9] A. Czajka, "Database of iris printouts and its application: Development of liveness detection method for iris recognition," in *Methods and Models in Automation and Robotics (MMAR), 2013 18th International Conference on*, 2013, pp. 28-33.

[10] O. V. Komogortsev and A. Karpov, "Liveness detection via oculomotor plant characteristics: Attack of mechanical replicas," in *Biometrics (ICB), 2013 International Conference on*, 2013, pp. 1-8.

[11] *LivDet-Iris: Liveness Detection-Iris Competition 2013 (part of IEEE International Conference on Biometrics: Theory, Applications and Systems, BTAS 2013)*. Available: http://people.clarkson.edu/projects/biosal/iris

[12] L. Ghiani, D. Yambay, V. Mura, S. Tocco, G. L. Marcialis, F. Roli*, et al.*, "LivDet 2013 Fingerprint Liveness Detection Competition 2013," in *Biometrics (ICB), 2013 International Conference on*, 2013, pp. 1-6.

[13] I. Chingovska, J. Yang, Z. Lei, D. Yi, S. Z. Li, O. Kahm*, et al.*, "The 2nd competition on counter measures to 2D face spoofing attacks," in *Biometrics (ICB), 2013 International Conference on*, 2013, pp. 1-6.

[14] J. Ortiz-Lopez, J. Galbally, J. Fierrez, and J. Ortega-Garcia, "Predicting iris vulnerability to direct attacks based on quality related features," in *Security Technology (ICCST), 2011 IEEE International Carnahan Conference on*, 2011, pp. 1-6.

[15] O. V. Komogortsev, C. Holland, A. Karpov, and H. Proença, "Multimodal Ocular Biometrics Approach: A Feasibility Study," in *IEEE Fifth International Conference on Biometrics: Theory, Applications and Systems (BTAS 2012)*, 2012, pp. 1-8.

[16] D. W. Hansen and J. Qiang, "In the Eye of the Beholder: A Survey of Models for Eyes and Gaze," *Pattern Analysis and Machine Intelligence, IEEE Transactions on,* vol. 32, pp. 478-500, 2010.

[17] E. D. Guestrin and E. Eizenman, "General theory of remote gaze estimation using the pupil center and corneal reflections," *Biomedical Engineering, IEEE Transactions on,* vol. 53, pp. 1124-1133, 2006.

[18] D. M. Stampe, "Heuristic filtering and reliable calibration methods for video-based pupil-tracking systems," *Behavior Research Methods, Instruments, & Computers,* vol. 25, pp. 137-142, 1993.

[19] C. D. Holland and O. V. Komogortsev, "Complex eye movement pattern biometrics: Analyzing fixations and saccades," in *Biometrics (ICB), 2013 International Conference on*, 2013, pp. 1-8.

[20] D. D. Salvucci and J. H. Goldberg, "Identifying fixations and saccades in eye-tracking protocols," presented at the Proceedings of the 2000 symposium on Eye tracking research & applications, Palm Beach Gardens, Florida, USA, 2000.

[21] *EyeLink. EyeLink 1000 Eye Tracker*. Available: http://www.sr-research.com/

[22] *CMITech. BMT-20 Iris Recognition System.* Available: http://www.cmi-tech.com/